The important but weakening maize yield benefit of grain filling prolongation in the US Midwest

Peng Zhu, Zhenong Jin, Qianlai Zhuang, Philippe Ciais, Carl Bernacchi, Xuhui Wang, David Makowski, David Lobell

MR. PENG ZHU (Orcid ID : 0000-0001-7835-3971)

DR. ZHENONG JIN (Orcid ID : 0000-0002-1252-2514)

Article type : Primary Research Articles

The important but weakening maize yield benefit of grain filling prolongation in the US Midwest

Peng Zhu[1], Zhenong Jin[1,2], Qianlai Zhuang[1,3], Philippe Ciais[4], Carl Bernacchi[5,6], Xuhui Wang[4], David Makowski[7], David Lobell[2]

1. Department of Earth, Atmospheric, and Planetary Sciences, Purdue University, West Lafayette, Indiana 47907 USA

2. Department of Earth System Science, Center on Food Security and the Environment, Stanford University, Stanford, CA, USA

3. Department of Agronomy, Purdue University, West Lafayette, Indiana 47907 USA

4. Laboratoire des Sciences du Climat et de l'Environnement (LSCE), CEA CNRS UVSQ, 91191 Gif-sur-Yvette, France

5. Department of Plant Biology, University of Illinois at Urbana-Champaign, Urbana, IL 61801, USA

6. Global Change and Photosynthesis Research Unit, USDA-ARS, Urbana, IL 61801, USA

7. UMR 211 Agronomie INRA, Agroparistech, Université Paris-Saclay, 78850 Thiverval-Grignon, France

Correspondence: Qianlai Zhuang, tel. +1 765 494 9610, fax +1 765 496 1210, e-mail: qzhuang@purdue.edu

Running head: Yield benefit of longer grain filling period

Keywords: Maize grain filling prolongation, US Midwest, yield benefit, crop model, crop growth stages, satellite data, global warming, food security

Abstract

A better understanding of recent crop yield trends is necessary for improving the yield and maintaining food security. Several possible mechanisms have been investigated recently in order to explain the steady growth in maize yield over the US Corn-Belt, but a substantial fraction of the increasing trend remains elusive. In this study, trends in grain filling period (GFP) were identified and their relations with maize yield increase were further analyzed. By using satellite data from 2000 to 2015, an average lengthening of GFP of 0.37 days per year was found over the region, which probably results from variety renewal. Statistical analysis suggests that longer GFP accounted for roughly one-quarter (23%) of the yield increase trend by promoting kernel dry matter accumulation, yet had less yield benefit in hotter counties. Both official survey data and crop model simulations estimated a similar contribution of GFP trend to yield. If growing degree days that determines the GFP continues to prolong at the current rate for the next 50 years, yield reduction will be lessened with 25% and 18% longer GFP under Representative Concentration Pathway 2.6 (RCP 2.6) and RCP 6.0, respectively. However, this level of progress is insufficient to offset yield losses in future climates, because drought and heat stress during the GFP will become more

prevalent and severe. This study highlights the need to devise multiple effective adaptation strategies to withstand the upcoming challenges in food security.

Introduction

Agricultural systems in many regions may be negatively impacted by increasing temperature especially when accounting for the nonlinear effect of climate extremes such as heat waves and droughts (Rattalino and Otegui, 2013; Porter and Semenov, 2005; Sánchez *et al.*, 2014; Schlenker and Roberts, 2009), which are predicted to become increasingly frequent in a warmer climate. Higher-than-optimal temperature negatively impacts maize yield through affecting reproductive structures (Siebers *et al.*, 2015; Siebers *et al.*, 2017), decreasing the Rubisco activation (Crafts-Brandner, 2002), and increasing water stress (Lobell *et al.*, 2013). Thus, to maintain or potentially increase productivity, agricultural systems must adapt to upcoming warmer and more extreme climates.

As the world's largest producer of maize, the US has seen a steady increase in maize yield since the 1950s through improvements in agronomic practices, genetic technology and favorable growing conditions despite interannual yield variability related to hot and dry summers (USDA, 2015). Several possible mechanisms have been investigated in order to understand this increasing trend in yields, including: expansion of more heat tolerant cultivars (Driedonks *et al.*, 2016), delayed foliar senescence or stay-green traits (Thomas and Ougham, 2014), new cultivars adapted to higher sowing density (Duvick, 2005; Tollenaar and Wu, 1999), development of pest resistant maize cultivars through genetically engineering (NRC, 2010), enhanced water use efficiency under rising atmospheric CO_2 (Lobell and Field, 2008; Jin *et al.*, 2017), and increase in accumulated solar radiation during the post-flowering phase (Tollenaar *et al.*, 2017). A drought sensitivity analysis over the US Midwest based on field maize yield data showed, however, higher sowing density brought about side effect that field maize yield sensitivity to water stress became increased

(Lobell *et al.*, 2014). In this context, it is necessary to understand the response of maize yield in farmers' fields to climate variation over time and thereby allowing crops more effectively to adapt to the future climate change.

Crop phenological development is essential for agricultural management practices (Irmak *et al.*, 2000), and reflects the combined effect of climate exposure and plant physiological traits (McMaster *et al.*, 2005). Specifically, this study focused on GFP, a critical kernel development stage when plant growth and grain formation is sensitive to stress (Badu-Apraku, 1983; Çakir, 2004; Cheikh, 1994). In addition, because there is a tight positive correlation between the grain filling length (GFL) and the final crop yield (Tollenaar *et al.*, 2017; Badu-Apraku, 1983), characterizing recent trends in GFL may also help explain yield trends.

Satellite remote sensing observations such as the vegetation index derived from moderate-resolution imaging spectroradiometer (MODIS) reflectance data provide the opportunity to characterize the regional-scale spatiotemporal patterns of field crop growth status information, in particular phenological transition dates (Sakamoto *et al.*, 2010). We used this long-term satellite data to generate spatially-explicit maize phenological date fields. Maize phenological information was then integrated with a crop model to understand the relationship between GFP trend and yield increase in the historic period. Finally, the implication of longer maturity variety for sustaining maize production under future climate scenarios was investigated.

Materials and Methods

In this study, 8-day Wide Dynamic Range Vegetation Index (WDRVI) derived from MODIS reflectance data (MOD09Q1 and MYD09Q1) from 2000 to 2015 was used to map trends in maize phenology in Illinois, Indiana, Iowa, Nebraska across the US Midwest, which collectively account for half of the total US maize production. Maize yield keeps growing across the four states at the rate of 1.4% per year during this

period (Fig. 1). To extract maize phenology, shape model fitting (SMF) has been shown as an effective approach and was validated at both site and state level (Sakamoto *et al.*, 2010; Sakamoto *et al.*, 2014; Zeng *et al.*, 2016). On the other hand, threshold based methods can be used to extract the starting and ending of growing season more flexibly. Thus, we developed and implemented a hybrid method combining SMF and threshold-based analysis to generate 8 million samples of maize phenological date from MODIS WDRVI data at 250×250 m spatial resolution from 2000 to 2015.

Satellite data. In this study, the 8-day time series of 250 m daily surface reflectance MODIS data on board Earth Observing System (EOS) Terra and Aqua satellite platforms: MOD09Q1 (2000-2015) and MYD09Q1 (2002-2015) Collection 6, was used. Four tiles MODIS data (h10v04, h11v04, h10v05, h11v05) covering the study area (4 states: Indiana, Illinois, Iowa, Nebraska) were downloaded from NASA Land Processes Distributed Active Archive Center. Although the daily satellite observations can better capture the phenological phase transition during maize growth, the 8-day composite products in MOD09Q1 and MYD09Q1 were selected to minimize the impact of clouds and haze. Generally, the MODIS 8-day composite products were systematically corrected for the effects of aerosol light scattering (Vermote and Vermeulen, 1999). Meanwhile, the constrained view-angle maximum value composite method guarantees the quality of surface spectral reflectance data for each 8-day period (Huete *et al.*, 2002). Both 250m MOD09Q1 and MYD09Q1 data consists of red (R) and near-infrared (NIR) bands with an actual spatial resolution of 231.7 m. Here a scaled WDRVI (Wide Dynamic Range Vegetation Index), generated by combining Terra and Aqua observations, is used to monitor the growing status of maize plants (Zeng *et al.*, 2016), because WDRVI is supposed to have a better performance in characterizing seasonal biomass dynamics than normalized difference vegetation index (NDVI), which is often saturated for dense vegetation and a linear relationship was identified between WDRVI and the green leaf area index (LAI) of both maize and soybean (Gitelson, 2004; Gitelson *et al.*, 2007). The scaled WDRVI is

calculated with the following equation:

$$\text{WDRVI}=100 * \frac{[(\alpha-1)+(\alpha+1)\times \text{NDVI}]}{[(\alpha+1)+(\alpha-1)\times \text{NDVI}]} \quad (1)$$

$$NDVI = (\rho_{NIR} - \rho_{red})/(\rho_{NIR} + \rho_{red}) \quad (2)$$

Where ρ_{red} and ρ_{NIR} are the MODIS surface reflectance in the red and NIR bands, respectively. A comparison of multiple vegetation indexes indicates WDRVI with α=0.1 showed a strong linear correlation with corn green LAI (Guindin-Garcia *et al.*, 2012). Here we also set α as 0.1 for WDRVI calculation. Before WDRVI calculation, the reflectance data were quality-filtered using the band quality control flags. Only the data passing the highest quality control test is retained.

Crop location information. A cropland dynamic layer (CDL) spanning from 2000 to 2015 generated by USDA/NASS was used to be as maize mask (The time span of NASS-CDL for Nebraska is from 2001 to 2015). The spatial resolution of the original products of NASS-CDL varied from year to year due to different satellite data being used. The satellite data sets used to generate NASS-CDL over 2000–2005 and 2010-2015 were obtained from Landsat/TM with 30 m resolution. Those used to generate NASS-CDL over 2006–2009 were obtained from Resourcesat-1/AWiFS with 56 m resolution. The CDL data was firstly projected to MODIS sinusoidal projection and then aggregated to 231.7 m. We only extracted the phenological information over the MODIS pixels with the corresponding maize fraction surpassing 80% determined by CDL aggregation, which can thus suppress the mixing effect of other vegetation types like grasses and soybean. The classification errors in the CDL data might mix non-crops signal into the WDRVI calculation. However, previous study showed that the influence of classification errors on maize phenological extraction can be minimized at regional scale (Sakamoto *et al.*, 2014), especially when a high threshold value (here it is 80%) was applied to filter mixing pixels.

Maize phenology and yield statistics data. USDA/NASS surveys crop progress and condition based on questionnaires and publishes percent complete (area ratio) of crop

fields that have either reached or completed a specific phenological stage, on Agricultural Statistics Districts (ASD) or state level, in a weekly report called the Crop Progress Report (CPR). The state level phenology information is available in the USDA/NASS Quick Stats 2.0 database. This weekly reported area ratios were interpolated using sigmoid function. The target phenological stages (emerged, silking, dent, and mature stages) were then determined as the date when the interpolated area ratio reached 50% on a state level (Tollenaar *et al.,* 2017). The phenological dates from CPR were used as a reference to evaluate the MODIS based estimations.

The county-level corn grain yield data covering the 4 states (IL, IN, IA, NE) were obtained from the Quick Stats 2.0 database. The selected data period was from 2000 to 2015. The unit system for corn grain yield is bushel per acre (bu/ac).

Climate data. Daily precipitation, minimum and maximum temperatures and relative humidity data at 4km resolution was obtained from University of Idaho Gridded Surface Meteorological Data (Abatzoglou, 2013) (http://metdata.northwestknowledge.net/). It is a gridded product covering the US continent and spanning from 1979 to 2016. This dataset is created by combining attributes of two datasets: temporally rich data from the North American Land Data Assimilation System Phase 2 (Mitchell, 2004) (NLDAS-2), and spatially rich data from the Parameter-elevation Regressions on Independent Slopes Model (Daly *et al.,* 2008) (PRISM). After validated using extensive network of weather stations across the United States, this dataset is proved to be suitable for landscape-scale ecological model. To be consistent with the climate data resolution, MODIS derived maize phenology information is aggregated to 4 km by averaging all available maize phenological date. Then the climate variables like mean temperature, mean VPD and mean precipitation during the vegetative period, grain filling period and total growth period are estimated by integrating daily climate data over the corresponding period according to MODIS derived phase starting and ending date. VPD is estimated from relative humidity and temperature data.

193 Here GDD, a commonly used metric as the cumulative thermal requirement for a crop
194 having experienced over the growing season for maize, is calculated from daily
195 temperature values. It is defined as the sum of all daily average temperatures over the
196 growing season in excess of 8 °C. A base temperature of 8 °C and a maximum
197 temperature of 35 °C for maize were used (Kiniry and Bonhomme, 1991). Specifically,
198 GDDcrit was used to refer to the GDD requirement from start grain filling to
199 maturity.

200 **Maize growing phase extraction.** A shape model fitting (SMF) (Fig. 2), which
201 represents the general pattern of corn growth characterized by time-series WDRVI,
202 was created using a similar procedure as previous study (Sakamoto *et al.*, 2010). The
203 shape model was defined by averaging 10 years (2001 to 2010) of 8 days WDRVI
204 observations from the irrigated continuous corn field at Mead, Nebraska operated by
205 the University of Nebraska Agricultural Research and Development Center. Then, the
206 shape model was geometrically scaled and fitted to 8-day time series WDRVI data
207 using the following equation:
208 $$h(x)=yscale\times\{g(xscale\times(x+tshift))\}, \quad (3)$$
209
210 where the function g(x) refers to the preliminarily defined shape model function and x
211 refers to WDRVI acquiring date. The function h(x) is transformed from the shape
212 model g(x) in time- and VI-axis directions with the scaling parameters xscale, yscale,
213 and tshift. The scaling parameters were optimally estimated by using ‘fminsearch’
214 function in Matlab R2015b to minimize the discrepancy between the scaled shape
215 model h(x) and the WDRVI data. Here the root mean square error (RMSE) between
216 the scaled shape model h(x) and the WDRVI data is used to quantify the discrepancy.
217 The dates of these key phenological stages, including emerged, silking, dent, and
218 mature date, were determined from satellite data by optimizing the dates of emerged,
219 silking, dent, and mature stages, given the pre-defined dates. Dent stage is about 35 to
220 42 days after silking when 'milk line' gets close to the dent end of the kernel. Maturity
221 date is about 55 to 65 days after silking and kernel dry weight reaches its maximum

(Abendroth et al. 2011). In the original study (Sakamoto et al., 2010), the pre-defined dates were empirically determined based on the ground-based phenology observations and were set as 150, 200, 240 and 265 day of year of the reference growing season, respectively. These parameters are also used in this study.

Although the previous study showed SMF had a good estimation of corn phenology at site and state level with RMSE of maize phenological stage estimation at ASD-level ranging from 1.6 (silking date) to 5.6 days (dent date) (Zeng *et al.*, 2016), there is an inevitable problem in this method that the linear scaling strategy with only two parameters (xscale and tshift) is too stiff and leads to identical trends in the 4 critical phenological dates. However, the US maize plants seems to have different or even opposite temporal shifts in different phenological dates as reported by Sacks and Kucharik (2011) like an advance in planting and emergence date while delay in maturity date during 1981-2005. Thus, a more flexible way to characterize the different trends in the four phenological dates is needed.

Among the numerous methods for deriving seasonal parameters from the time-series vegetation index, the threshold method, which assumes that a specific phenology will start when the vegetation index value exceeds a threshold, is widely used because it generally keeps dates within a certain reasonable range and can achieve relatively high accuracies. In general, threshold is usually selected based on crop types. In this study, the WDRVI of 18 is set as threshold based on trials when comparing the estimation with NASS reported emergence date and maturity date for 4 states. We used a hybrid method by merging the advantage of SMF in extracting the silking and dent dates and the threshold method in extracting the growing start (emergence) and ending (maturity) date (Fig. 2). Furthermore, SMF was restricted to only fit WDRVI curve for a specific range, where WDRVI is above its 40% peak value, so the estimated parameters are mainly relevant to the silking and denting phenological information. Before applying the threshold method, the WDRVI curve is firstly smoothed using a robust smoothing-spline approach to reduce the signal

noise (Keenan *et al.*, 2014). To minimize the impact of maize pixels contaminated by clouds, cloud shadow and aerosol loading, a 3*3 windows is used to filter the data. In each 3*3 windows, only those with more than 4 maize pixels were selected for phenology extraction, so there were multiple observational vegetation index data to constrain the optimization model, which can thus improve the stability of parameters estimation. In addition, the searching boundary for the scaling parameter yscale and xscale was empirically set as [0.4, 1.8] to ensure the extracted phenological date within a reasonable range. Finally, approximate 8 million grids containing the 4 critical phenological date over 16 years were retrieved. When the MODIS extracted emergence date was aggregated to the state level and compared with the NASS CPR, we found a systematic bias in emergence dates that MODIS estimated emergence dates were 7.6 days later than the NASS report date. This systematic bias might result from the selection of WDRVI threshold. Then this systematic bias was deducted from the MODIS derived emergence date before comparison. Nevertheless, the bias will not influence the estimation of grain filling starting and ending date. The state level comparisons show a good agreement for the four key phenological stages with the RMSE ranging from 1.6 (silking date) to 4.4 days (dent date) (Table 1).

Finally, the GFP and grain filling GDDcrit trend was analyzed in 4km grid cell to keep consistent with the spatial resolution of climate data. This larger grid size than the orignal resolution of MODIS data (250m) brings more phenological samples for trend analysis, thus a stronger statistical inference can be made.

Yield stability and GFP. Generalized additive regression model (GAM), an effective and flexible method to characterize nonlinear effects of explanatory variables, was used here to explore the relationship between yield stability and GFP. Coefficient of variation and standard deviation of county yield over time were alternatively used to represent the temporal stability of maize yield. The model was constructed based on R package "mgcv" (Wood, 2006). The spline method was used as the smooth term. In addition to GFP, climatic variables including multi-year mean precipitation, mean

daily temperature and vapor pressure deficit (VPD) during GFP over 2000-2015 were also selected as the covariates. Both county level GFP and the trends in GFP were alternately used as the explanatory variables, so the influence of the longer GFP in space and GFP extension over time on yield stability was explored.

Crop model simulations. An agricultural system modeling platform APSIM version 7.7 is used here to simulate the benefit of GFP extension under future climate. APSIM can simulate a number of crops under different climatic and management conditions, and hence is used worldwide to address a range of research questions related to cropping systems (Holzworth *et al.,* 2014). In particular, maize is simulated by the APSIM-Maize module. The APSIM-Maize module is inherited from the CERESMaize, with some modifications on the stress representation, biomass accumulation and phenological development (Hammer *et al.,* 2010). This flexible process-based model allows us to separately estimate the yield benefit of agronomic practices like the cultivar shift indicated by higher thermal time requirement during grain fillling.

The MODIS data showed both the grain filling GDD_{crit} and GFP increased, suggesting the GFP extension is likely to be associated with variety change, such as the adoption of longer maturity variety. We designed three simulations to explore the contribution of GFP extension to recent decades yield increase. All of the simulations were forced with University of Idaho Gridded Surface Meteorological Data from 2000 to 2015. The parameter in APSIM, phase_tt(start_to_end_grain), defining the GDD requirement from start grain filling to maturity was increased to drive a prolonged GFP to emulate the adoption of longer maturity variety over this period. Simulation sim1 is the control with no increase in variety GDD_{crit}; simulation sim2 sets an increase in variety GDD_{crit} by 0.65% per year which charasterized the observed increasing rate in all counties; simulation sim3 sets an increase in GDD_{crit} by 0.82% per year which represented the observed increasing rate in GFP prolonged counties. The soil parameters, like soil hydraulic properties and soil organic matter

fractions were extracted from the State Soil Geographic (STATSGO) data base, as collected by the National Cooperative Soil Survey over the course of a century. For each simulation grid, the soil information was queried through R package 'soil DB' (http://ncss-tech.github.io/AQP/). Management information like planting density and fertilizer application amount was taken from the USDA NASS survey report at state level. Crop sowing date was derived from the Crop Calendar Dataset (Sacks *et al.*, 2010). We used generic maize hybrids ('B_110') provided by APSIM version 7.7 to run the simulation.

To investigate the yield benefit of longer GFP until 2060-2070, we constructed two simulations for climate forcing data from historic (2000-2015) period and two future climate scenarios (RCP2.6 and RCP6.0), respectively: one is the control simulation, where the maize GDD_{crit} was set as a constant using generic cultivar parameters ('B_110'); the other one is the GFP prolonged simulation, where GDD_{crit} was increased by 0.82% per year to be consistent with the current advance in maize cultivar based on historical MODIS image analysis. For the historic period simulation, the climate forcing data during 2000-2015 was recycled until 2070. For the future climate scenarios, three climate forcing data was used to account for the climate model uncertainty in global temperature: Institute Pierre Simon Laplace CM5A Earth system model (IPSL-CM5A-LR), Geophysical Fluid Dynamics Laboratory Earth System Model with Generalized Ocean Layer Dynamics component (GFDL-ESG2G) and the Hadley Centre Global Environment Model, version 2-Earth System (HadGEM2-ES). As a C_4 plant, maize plants loss less water in response to future enriched atmospheric CO_2, which is modeled by enhanced transpiration efficiency in APSIM. The CO_2 concentration is set as 380 ppm for the historic simulation while increased to follow the concentration trajectory defined in RCP2.6 and RCP6.0 (Meinshausen *et al.*, 2011). The soil parameters and management information here followed the previous simulations sim1 (sim2, sim3). Then yield increasing rate in 2060-2070 is calculated by (yield with prolonged GFP − yield in control simulation)/(yield in control simulation) with three climate forcing data: historic

342 period, RCP2.6 and RCP6.0.

343

344 **Conceptual model of GFP trend analysis.** GDD during GFP can be generally
345 written as:

346 $$GDD_8^{35} = \int_{silking}^{maturity} DD_t, DD_t = \begin{cases} 0, when\ Tmean < 8 \\ Tmean - 8, when\ 8 \le Tmean < 35 \\ 27, when\ Tmean \ge 35 \end{cases} \quad (4)$$

347 8, 35 means the lower and upper bounds of daily mean temperature (Tmean) to
348 calculate GDD. As most of Tmean is within this range, it can be approximately
349 written as:

350 $$GDD_8^{35} \approx GFP \cdot (Tmean - 8) \quad (5)$$

351 Then the GFP trend can be rearranged as:

352 $$\frac{dGFP}{GFP \cdot dt} \approx \frac{dGDD}{GDD \cdot dt} - \frac{d(Tmean - 8)}{(Tmean - 8) \cdot dt} \quad (6)$$

353 So GFP trend ($\frac{dGFP}{GFP \cdot dt}$) can be approximately estimated by GDD trend minus
354 Tmean trend. As Tmean trend is very small (Fig. S4), GFP trend is mostly driven by
355 GDD trend.

356

357 **Yield benefit analysis using statistical method.** We conducted a panel analysis to
358 quantify the statistical contribution of increasing GFP to the observed increase of
359 maize yield. A linear model considering the fixed effects in each year and county was
360 used:

361 $$log(Yield_{i,t}) = \beta_1 * GFP_{i,t} + Year_t + County_i + \varepsilon_{i,t} \quad (7)$$

362 where $Year_t$ *and* $County_i$ specify independent intercept of each year and county.

363

364 **Results and Discussion**

365 The verification at state level showed a good agreement between MODIS derived
366 maize phenology and the National Agricultural Statistics Service (NASS) reported

state mean phenological dates for the four key maize growth stages of emergence (late May), silking (Middle July), dent (late August) and maturity (late September) (Fig. 3). The root mean square error (RMSE) of the 4 phenological dates estimated over the four states ranged from 1.6 days (silking date in Nebraska) to 4.4 days (dent date in Nebraska) (Table 1). The duration between emergence and maturity is used to represent maize total growth period, and the duration between silking and maturity dates is used to define the GFP. Across the four states, GFP generally starts from around day of year (DOY) 200 and ends by DOY 260 but varied interannually (Fig. 3).

GFP trend was analyzed on a 4km grid to keep consistent with the spatial resolution of climate data (Abatzoglou, 2013). We found there were significant trends of maize phenology, with silking dates becoming earlier in 61% of the pixels and more pixels (84%) exhibiting a later maturity date (Fig. S2). This resulted in a significant extension of the GFP over 81% of the pixels during the 16-year analysis (Fig. S2). This trend of GFP obtained from satellite data is similar to NASS reports when aggregated to state level (Fig. 4). This is also in line with the study over the U.S. Corn Belt from Sacks and Kucharik (Sacks and Kucharik, 2011) that was conducted for the earlier period of 1981-2005 based on NASS state reports.

The spatial variation of the GFP trends shows increasing trends in most Midwest areas and decreasing trends in drier areas like western Nebraska (Fig. 5a). The spatial mean of the GFP trends across the four states is 0.37 days per year with interquartile values ranging from 0.09 to 0.68 (Fig. 5b). When aggregated to the county level, 79% of the counties exhibit a significant increase in GFP (Fig. 5a). As the longer GFP might be a result of increased variety thermal time accumulation, we also looked into growing degree days (GDD). GDD is a commonly used metric to measure thermal time accumulation of crops and the critical threshold GDD_{crit} at which GFP is fulfilled is an important physiological trait of maize cultivars. The GDD_{crit} calculated from satellite and climate data shows trends that have a similar spatial structure than the

GFP trends, with a mean rate of increase of 0.65% per year (Fig. 5c and d). The small warming trend observed in the study area (Fig. S4) would have shortened GFP (Egli, 2004), if GDD_{crit} keeps constant. Thus the observed longer GFP is likely to be associated with variety shifts, marked by the concurrently increasing GDD_{crit}. As GDD_{crit} reflects the thermal time requirement of a specific cultivar to achieve grain filling, the increasing GDD_{crit} over time (Fig. 5c) and the higher GDD requirement from emergence to maturity in south counties with warmer temperature (Fig. 6 and Fig. S5) suggest that farmers have switched to use longer maturity cultivars to compensate for the negative impact of warmer temperatures which otherwise shorten the overall growing season length and the GFP (Çakir *et al.*, 2004; Dwyer *et al.*, 1994; Egli, 2004; Sacks and Kucharik, 2011).

Evidence from agronomical research shows that extended GFP contributes a higher yield by providing more time to translocate photosynthates to kernels (Crosbie and Mock., 1981; Wang *et al.*, 1999). With equation (7), the estimated yield benefit β_1 (% per day) defining the sensitivity of yield to GFP is $0.86 \pm 0.03\%$ ($\pm$standard error, SE), indicating that one additional day of GFP increased maize yield on average by 0.86%. According to this empirical relationship and the estimated total yield trend (1.4% per year), the lengthening of GFP observed in the MODIS data is inferred to have contributed to $23 \pm 0.7\%$ ($\pm$SE) of the maize yield trend for all of the studied counties (Fig. 7a). This contribution was computed as:

$$\text{Contribution} = \beta_1 \times \text{GFP increasing trend / Yield increasing trend} \quad (8)$$

Equation (8) was also applied to the NASS reported maize phenological data at state level. In this application, the fixed effect term $County_i$ for each county was replaced with the state fixed effect $State_i$, and the estimated value of β_1 was slightly higher ($1.08 \pm 0.18\%$ per days) compared to the above estimation (Fig. 7a). Given the mean GFP trend (0.43 ± 0.12 days per year), which is also based on NASS report, this empirical estimation solely based on NASS report suggests GFP prolongation

contributed 31±4.8% of the maize yield trend, which is slightly higher than the above estimation based on satellite data analysis.

A previous study suggested the solar brightening during GFP is responsible for about 27% of the observed increase in US maize yield from 1984 to 2013 (Tollenaar *et al.*, 2017). However, we did not find a significant increase in solar radiation across the four corn states considered during the study period when using the same solar radiation dataset integrated over the grain filling period (Fig. S6).

When counties were grouped based on whether their GFP has increased or not, counties where GFP increased showed on average higher increasing rates of GDD_{crit} (0.82% per year) and grain yield (1.5% per year) compared to the mean of all the counties (Fig. 7b). According to the estimated β_1, the mean increase in GFP for those counties is estimated to have contributed to 27±0.8% (±SE) of the yield trend. Alternatively, counties with decreasing GFP trend, perhaps resulting from the effects of climatic warming overwhelming those of cultivars, showed a smaller yield trend of 1.0% per year (Fig. 7b). Alternatively, when equation (8) was applied to counties grouped by warmer and cooler growing season mean temperature separately, a significant ($p<0.01$) lower yield benefit (β_1) was found in warmer counties (Fig. 7b). This result implies that the yield benefit of GFP extension might be weakened in future warmer climate. This analysis also explained why the yield benefit in GFP prolonged counties was higher than the one estimated in GFP shortened counties (Fig. 7b), since these counties generally have a warmer background climate (Fig. S8).

To account for possible omitted variables in the above analysis, for instance if an unobserved factor such as pest resistance affects both GFP and yield on a year-to-year basis, we also conducted a regression comparing linear yield trends with GFP trends over the study period as follows:

$$Yield\ trend_i = \beta_1 * GFP\ trend_i + \varepsilon_i \quad (9)$$

where i is the county indices. In this model, the effect of year-to-year variation in each

county is minimized, thus the significant slope (0.82% per day) primarily quantifies the contribution of GFP trend to yield trend (Fig. 7c), which was close to the one of the panel analysis (0.86% per day). The intercept term in this regression (1.1% per years) indicates the yield trend with no GFP extension and is 27% lower than the trends of GFP extended counties (1.5% per year), which is also consistent with the above estimation.

To further guard against the impact of potential confounding factors which might be not fully separated in the statistical models, the process-based crop model APSIM was then applied to simulate the contribution of GFP extension to yield trend. In this analysis, the variety GDD_{crit} parameter of the model was increased to simulate the observed variety shift caused GFP extension. Three simulations were conducted: sim1 has no increase in GDD_{crit}; sim2 assumes an increase GDD_{crit} of 0.65% per year from the observed mean GDD_{crit} trend in all counties; sim3 sets a larger increase of GDD_{crit} of 0.82% per year consistent with observed mean GDD_{crit} trend over a subset of counties showing significant GFP increase. Compared to the results of sim1, the modelled increasing trends of GFP in sim2 and sim3 were close to the observed GFP trend (Fig. 8). The yield increase in sim2 and sim3 attributable to GDD_{crit} presents a positive trend of 0.24% and 0.34% per year, respectively (Fig. 9), which thus produces a close estimation of the contribution of GFP extension to yield trend (Table 2). The results from sim1 also confirm that the GFP extension was caused by shift in varieties because the GFP is shortened by climatic warming where there is no increase in variety GDD_{crit} (Fig. 8).

Climate change is also expected to exacerbate the variability of crop yields (Ray *et al.*, 2015; Wheeler and Braun, 2013). Therefore, we analyzed the influence of a prolonged GFP on yield stability, another important dimension of food security (Campbell *et al.*, 2016). We used the coefficient of variation (CV) of yield in each county during 2000-2015 as an index of stability. A generalized additive regression model (GAM), suitable to account for nonlinear effects of explanatory variables, was employed to

relate yield CV with GFP. We found that a longer GFP (Fig. 10a) and an increase of GFP over time (Fig. 10b) correspond to lower CV of yield when accounting for the climatic covariates, suggesting that longer GFP in both space and time is associated with more stable yields. The reason might be that the selection of longer GFP cultivars is associated with increasing stress tolerance and thereby reduces the negative impact of warming on yield stability (Tollenaar and Lee, 2002).

Finally, the APSIM model was used to investigate the future benefit of maize production across the US Midwest with three ensembles of future climate forcing data to account for the climate model uncertainty in global temperature. The simulations for the next 50 years suggest that if farmers are able to switch to longer maturity variety (at the GDD_{crit} current rate of 0.82% per year), the maize GFP in 2060-2070 will be lengthened by 25% and 18% under the RCP 2.6 and RCP 6.0 (Fig. 11a), respectively. This means an approximate 15 days extension of GFP under the RCP 2.6, so the future maturity date still falls in a reasonable period for harvesting in these simulations. Simulations indicate that a continuation of the GFP prolongation rate would continue to benefit yields (Fig. 11b), albeit by a smaller amount in future climate conditions compared to the historic period (Fig. 11c). Specifically, the predicted 10.8% and 13.6% yield loss under RCP 2.6 and RCP 6.0 could be partially offset by longer GFP, with a benefit of 7.2% and 5.6% under RCP 2.6 and RCP 6.0, respectively. The reduced benefit of GFP results in part from the increasing water and heat stress under a future warmer climate (Fig. S9), which could decrease yield significantly during maize grain formation (Siebers *et al.*, 2017).

Overall, we found there was a significant GFP extension and concurrent increasing GDD_{crit} during the last 16 years across the U.S. Midwest Corn Belt, which is likely to reflect changes in the traits of maize cultivars. The GFP prolongation shows the potential to increase the maize yield and also to stabilize the yield variability but its yield benefit might diminish under future warmer climate. Although the GFP information extracted here is mainly based on satellite observed canopy chlorophyll

content but not on ground identified kernel color development, this method estimated a similar GFP trend and contribution of GFP prolongation to yield increase across the US Midwest when compared with the state level statistical data and more importantly it provided more detailed spatial information. Our study suggests that the historic satellite data can be utilized to map field crop phenological traits at large scales with fine spatial resolution to understand how farm management influence yield trend and the climatic response of crop growth at specific stage. When the observed GFP prolongation rate is applied up to 2070, the negative impact of climatic warming is partially offset by lengthening the GFP, but the grain yield still decreased even in the mild emission climate scenario, highlighting multiple adaptation strategies are necessary for future agricultural management in the region.

Acknowledgments: We thank two anonymous reviewers' comments to help us significantly improve this study. This research was supported by a NSF project (IIS-1027955) and a NASA LCLUC project (NNX09AI26G) to Q. Z. We acknowledge the Rosen High Performance Computing Center at Purdue for computing support.

Reference

Abendroth, L., Elmore, R. W., Boyer, M., & Marlay, S. (2011) Corn growth and development.

Abatzoglou JT (2013) Development of gridded surface meteorological data for ecological applications and modelling. *International Journal of Climatology*, **33**, 121–131.

Badu-Apraku B, Hunter RB, Tollenaar M (1983) Effect of Temperature during Grain Filling on Whole Plant and Grain Yield in Maize (Zea mays L.). *Canadian Journal of Plant Science*, **63**, 357–363.

Çakir R (2004) Effect of water stress at different development stages on vegetative

544 and reproductive growth of corn. *Field Crops Research*, **89**, 1–16.
545 Campbell BM, Vermeulen SJ, Aggarwal PK *et al.* (2016) Reducing risks to food
546 security from climate change. *Global Food Security*, **11**, 0–1.
547 Cheikh N, Jones RJ (1994) Disruption of Maize Kernel Growth and Development by
548 Heat Stress (Role of Cytokinin/Abscisic Acid Balance). *Plant Physiology*, **106**,
549 45–51.
550 Crafts-Brandner SJ (2002) Sensitivity of Photosynthesis in a C4 Plant, Maize, to Heat
551 Stress. *Plant Physiology*, **129**, 1773–1780.
552 Crosbie, T. M., and J. J. Mock (1981) Changes in physiological traits associated with
553 grain yield improvement in three maize breeding programs. *Crop Science*, **21**,
554 255-259.
555 Daly C, Halbleib M, Smith JI *et al.* (2008) Physiographically sensitive mapping of
556 climatological temperature and precipitation across the conterminous United States.
557 *International Journal of Climatology*, **28**, 2031–2064.
558 Driedonks N, Rieu I, Vriezen WH (2016) Breeding for plant heat tolerance at
559 vegetative and reproductive stages. *Plant Reproduction*, **29**, 67–79.
560 Duvick DN (2005) The Contribution of Breeding to Yield Advances in maize (Zea
561 mays L.). *Advances in Agronomy*, **86**, 83–145.
562 Dwyer LM, Ma BL, Evenson L, Hamilton RI (1994) Maize physiological traits
563 related to grain yield and harvest moisture in mid- to short-season environments.
564 *Crop Science*, **34**, 985–992.
565 Egli DB (2004) Seed-fill duration and yield of grain crops. *Advances in Agronomy*, **83**,
566 243–279.
567 Gitelson AA (2004) Wide Dynamic Range Vegetation Index for Remote
568 Quantification of Biophysical Characteristics of Vegetation. *Journal of Plant*
569 *Physiology*, **161**, 165–173.
570 Gitelson AA, Schalles JF, Hladik CM (2007) Remote chlorophyll-a retrieval in turbid,
571 productive estuaries: Chesapeake Bay case study. *Remote Sensing of Environment*,
572 **109**, 464–472.
573 Guindin-Garcia N, Gitelson AA, Arkebauer TJ, Shanahan J, Weiss A (2012) An

574 evaluation of MODIS 8- and 16-day composite products for monitoring maize
575 green leaf area index. *Agricultural and Forest Meteorology*, **161**, 15–25.
576 Hammer GL, Van Oosterom E, McLean G, Chapman SC, Broad I, Harland P,
577 Muchow RC (2010) Adapting APSIM to model the physiology and genetics of
578 complex adaptive traits in field crops. *Journal of Experimental Botany*, **61**,
579 2185–2202.
580 Holzworth DP, Huth NI, deVoil PG *et al.* (2014) APSIM – Evolution towards a new
581 generation of agricultural systems simulation. *Environmental Modelling &*
582 *Software*, **62**, 327–350.
583 Huete A, Didan K, Miura T, Rodriguez EP, Gao X, Ferreira LG (2002) Overview of
584 the radiometric and biophysical performance of the MODIS vegetation indices.
585 *Remote Sensing of Environment*, **83**, 195–213.
586 Irmak S, Haman DZ, Bastug R (2000) Determination of crop water stress index for
587 irrigation timing and yield estimation of corn. *Agronomy Journal*, **92**, 1221–1227.
588 Jin Z, Ainsworth EA, Leakey ADB, Lobell DB (2018) Increasing drought and
589 diminishing benefits of elevated carbon dioxide for soybean yields across the US
590 Midwest. *Global Change Biology*, **24**, e522–e533.
591 Keenan TF, Gray J, Friedl MA *et al.* (2014) Net carbon uptake has increased through
592 warming-induced changes in temperate forest phenology. *Nature Climate Change*,
593 **4**, 598–604.
594 Kiniry, J. R., and R. Bonhomme. (1991) Predicting crop phenology **11**, 5-131.
595 Lobell DB, Hammer GL, McLean G, Messina C, Roberts MJ, Schlenker W (2013)
596 The critical role of extreme heat for maize production in the United States. *Nature*
597 *Climate Change*, **3**, 497–501.
598 Lobell DB, Field CB (2008) Estimation of the carbon dioxide (CO2) fertilization
599 effect using growth rate anomalies of CO2 and crop yields since 1961. *Global*
600 *Change Biology*, **14**, 39–45.
601 Lobell DB, Roberts MJ, Schlenker W, Braun N, Little BB, Rejesus RM, Hammer GL
602 (2014) Greater sensitivity to drought accompanies maize yield increase in the U.S.
603 Midwest. *Science*, **344**, 516–519.

McMaster GS (2005) Phytomers, phyllochrons, phenology and temperate cereal development. *Journal of Agricultural Science*, **143**, 137–150.

Meinshausen M, Smith SJ, Calvin K *et al.* (2011) The RCP greenhouse gas concentrations and their extensions from 1765 to 2300. *Climatic Change*, **109**, 213–241.

Mitchell KE (2004) The multi-institution North American Land Data Assimilation System (NLDAS): Utilizing multiple GCIP products and partners in a continental distributed hydrological modeling system. *Journal of Geophysical Research*, **109**, D07S90.

National Research Council (2010) The impact of genetically engineered crops on farm sustainability in the United States. *National Academies Press*.

Porter JR, Semenov MA (2005) Crop responses to climatic variation. *Philosophical Transactions of the Royal Society B-Biological Sciences*, **360**, 2021–2035.

Rattalino Edreira JI, Otegui ME (2013) Heat stress in temperate and tropical maize hybrids: A novel approach for assessing sources of kernel loss in field conditions. *Field Crops Research*, **142**, 58–67.

Ray DK, Gerber JS, Macdonald GK, West PC (2015) Climate variation explains a third of global crop yield variability. *Nature Communications*, **6**.

Sacks WJ, Deryng D, Foley JA, Ramankutty N (2010) Crop planting dates: An analysis of global patterns. *Global Ecology and Biogeography*, **19**, 607–620.

Sacks WJ, Kucharik CJ (2011) Crop management and phenology trends in the U.S. Corn Belt: Impacts on yields, evapotranspiration and energy balance. *Agricultural and Forest Meteorology*, **151**, 882–894.

Sakamoto T, Wardlow BD, Gitelson AA, Verma SB, Suyker AE, Arkebauer TJ (2010) A Two-Step Filtering approach for detecting maize and soybean phenology with time-series MODIS data. *Remote Sensing of Environment*, **114**, 2146–2159.

Sakamoto T, Gitelson AA, Arkebauer TJ (2014) Near real-time prediction of U.S. corn yields based on time-series MODIS data. *Remote Sensing of Environment*, **147**, 219–231.

Sánchez B, Rasmussen A, Porter JR (2014) Temperatures and the growth and

development of maize and rice: A review. *Global Change Biology*, **20**, 408–417.

Schlenker W, Roberts MJ (2009) Nonlinear temperature effects indicate severe damages to U.S. crop yields under climate change. *Proceedings of the National Academy of Sciences*, **106**, 15594–15598.

Siebers MH, Yendrek CR, Drag D *et al.* (2015) Heat waves imposed during early pod development in soybean (Glycine max) cause significant yield loss despite a rapid recovery from oxidative stress. *Global Change Biology*, **21**, 3114–3125.

Siebers MH, Slattery RA, Yendrek CR *et al.* (2017) Simulated heat waves during maize reproductive stages alter reproductive growth but have no lasting effect when applied during vegetative stages. *Agriculture, Ecosystems and Environment*, **240**, 162–170.

Thomas H, Ougham H (2014) The stay-green trait. *Journal of Experimental Botany*, **65**, 3889–3900.

Tollenaar M, Wu J (1999) Yield improvement in temperate maize is attributable to greater stress tolerance. *Crop Science*, **39**, 1597–1604.

Tollenaar M, Lee EA (2002) Yield potential, yield stability and stress tolerance in maize. *Field Crops Research*, **75**, 161–169.

Tollenaar M, Fridgen J, Tyagi P, Stackhouse PW, Kumudini S (2017) The contribution of solar brightening to the US maize yield trend. *Nature Climate Change*, **7**, 275–278.

USDA (2015) World Agricultural Supply and Demand Estimates. United States Department of Agriculture, 1–40.

Vermote EF, Vermeulen A (1999) Atmospheric correction algorithm: spectral reflectances (MOD09). ATBD version 4(April):1–107.

Wang G, Kang MS, Moreno O (1999) Genetic analyses of grain-filling rate and duration in maize. *Field Crops Research*, **61**, 211–222.

Wheeler T, von Braun J (2013) Climate change impacts on global food security. *Science*, **341**, 508–13.

Wood, S. N. (2006) Generalized additive models : an introduction with R. Texts Stat. Sci. xvii, 392.

664 Zeng L, Wardlow BD, Wang R, Shan J, Tadesse T, Hayes MJ, Li D (2016) A hybrid
665 approach for detecting corn and soybean phenology with time-series MODIS data.
666 *Remote Sensing of Environment*, **181**, 237–250.

667

668 **Tables**

669 Table1. RMSE (days) of 4 phenological stages estimation over four states

State	Emergence	Silking	Dent	Maturity
Illinois	4.0	1.9	2.8	3.4
Indiana	4.2	2.2	4.0	3.2
Iowa	2.9	4.3	3.3	3.6
Nebraska	3.1	1.6	4.4	3.0

670

671

672

673 Table2. Contribution of grain filling length extension to the maize yield increasing
674 trend estimated using APSIM (± indicates the SE)

	GFP prolonged counties	All counties
GDDcrit increasing rate (% per year)	0.82	0.65
Simulated yield increase rate (% per year)	0.34	0.24
Observed yield trend (% per year)	1.5±0.07	1.4±0.08
Contribution	23±1.6%	17±1.1%

675 **Figure captions**

676 **Figure 1.** (a) Trends in maize yield for each county, where the empty counties mean

677 that county has less than 12 years available data. (b) Mean maize yield increasing rate
678 for all counties. The error bars indicate the spatial variation of maize yield for all
679 counties.
680
681 **Figure 2.** The procedure of hybrid maize phenological extraction by merging shape
682 model fitting and threshold based method. The blue line is the spline approach
683 smoothed WDRVI time series data and the red line is the scaled shape model fitting
684 and the dashed blue line indicates the threshold, which is set as 18 based on trials
685 when compared with the NASS reported emergence and maturity date for 4 states.
686 The circle on red curve indicates the phenological date determined by shape model
687 fitting. Here the silking and dent dates were determined by shape model fitting and
688 the emergence and maturity date were determined by the threshold.
689
690 **Figure 3.** Comparison of maize phenological dates between NASS statistical data and
691 MODIS-derived estimation aggregated over state level. The two dashed lines in each
692 figure define the region where the errors between MODIS-derived estimation and
693 NASS statistical data are less than 5 days.
694
695 **Figure 4.** Time series of MODIS derived (blue) and NASS reported (red) silking and
696 maturity date for 4 states during 2000-2015. The lines show the GFL trend estimated
697 by the non-parametric Theil-Sen fitting.
698
699 **Figure 5.** Trends in county-level grain filling length and grain filling GDD
700 (GDD_{crit}), (a) and (c), where the empty counties mean that county has less than 12
701 years available data. For a specific year, a county with a number of maize grid cells
702 less than 100 is regarded as unavailable. When estimating the trend, all of the grid
703 cells in a county were pooled. And all of the trends shown are significant. The inset in
704 (a) indicates GFP trend for the 4 states derived from NASS report and satellite data.
705 The error bars indicate standard deviation of spatially estimated GFP trend. The
706 distribution of grain filling length and GDD_{crit} trend in each 4km grid, (b) and (d).

The grey horizontal line illustrates the mean trend of GDD_{crit} or grain filling length for all counties and the blue horizontal line illustrates the mean trend of GDD_{crit} or grain filling length for the counties where GFP has extended. GFP is defined as the period from silking to maturity. The grain filling length and GDD_{crit} trend was estimated by the non-parametric Theil-Sen fitting.

Figure 6. Scattering of county level (332 counties) multiple year mean GDD from emergence to maturity in temperature and precipitation space (points with black circles indicate the counties with irrigated area > 50%).

Figure 7. GFP trend, yield benefit of GFP prolongation and contribution of GFP prolongation to yield increase. (a) GFP trend, yield benefit (β_1) and GFP contribution to yield increase estimated from NASS report and MODIS derived maize phenological progress data. GFP contribution was computed as: $\beta_1 \times$ GFP increasing trend / Yield increasing trend. The scales for GFP contribution to yield increase are shown in right y-axis. (b) GDD_{crit} trend, yield trend and yield benefit of GFP extension (β_1) based on counties grouped by whether their GFP have prolonged or not. Yield benefit was also separately estimated by grouping growing season mean temperature. Warmer and cooler counties were divided according to the median value of growing season mean temperature. The yield benefit is then estimated by applying equation (8) to each group. The scales for yield benefit are shown in right y-axis. The error bars in (a) and (b) indicate the SD of each estimation. (c) The effect of GFP trend on maize yield trend. Each point corresponds to one county's trend in GFP and yield during 2000-2015.

Figure 8. Simulated grain filling length to explore the contribution of grain filling length to the growing maize yield using APSIM 7.7. sim1 is the control without grain filling prolongation; sim2 is to increase GDD_{crit} by 0.65% per year to characterize the observed GDD_{crit} trend in all counties; sim3 is to increase GDD_{crit} by 0.82% per year to characterize observation of GFP prolonged counties. The left panel shows the mean

737 time series of GFL in simulation 1 and the right panel shows the GFL difference.

738

739 **Figure 9.** APSIM 7.7 simulated maize grain yield with different rate of GFP
740 prolongation to explore the contribution of grain filling length to growing maize yield.

741

742 **Figure 10.** The effect of grain filling length on maize yield stability. Coefficient of
743 variation (CV) of the yield in each county over 2000-2015 as a function of (a) the
744 multi-year mean grain filling length, and (b) the trend of the grain filling period. Both
745 longer GFP across different counties in space (a) and time (b) are associated with a
746 smaller CV of yield, that is, more stable yields. The shaded areas indicate the 95%
747 confidence interval. Each small bar next to the horizontal line is a value observed for
748 a county.

749

750 **Figure 11.** The benefit of prolonged grain filling period for maize yield in future
751 climate. Boxplot of grain filling length (a) and maize yield (b) simulated with the
752 APSIM model running up to 2060-2070 assuming constant (yellow) or linearly
753 increasing GDD_{crit} at the same rate than during the past 16 years (blue) in comparison
754 with the historic period 2000-2015. (c) Comparison of maize yield benefit with
755 GDD_{crit} increase at the rate of 0.82% per year in historic and future climate conditions.
756 Here yield increasing rate up to 2060-2070 is calculated by (yield with prolonged
757 GDD_{crit} − yield with constant GDD_{crit})/(yield with constant GDD_{crit}) using three
758 climate forcing data: 2000-2015, RCP2.6, RCP6.0 (see Method). The lines in the
759 middle of box represent median projection, boxes show the interquartile range, and
760 whiskers indicate the 5th–95th percentile of projections.

761

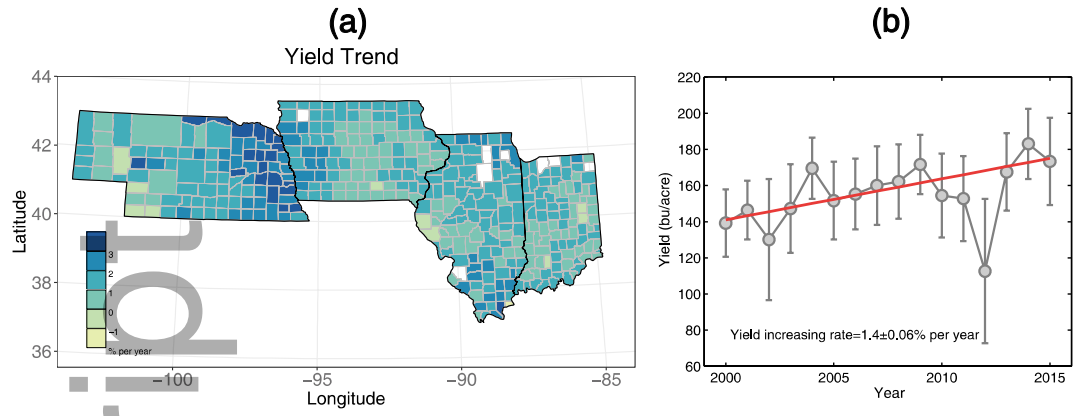

762

763

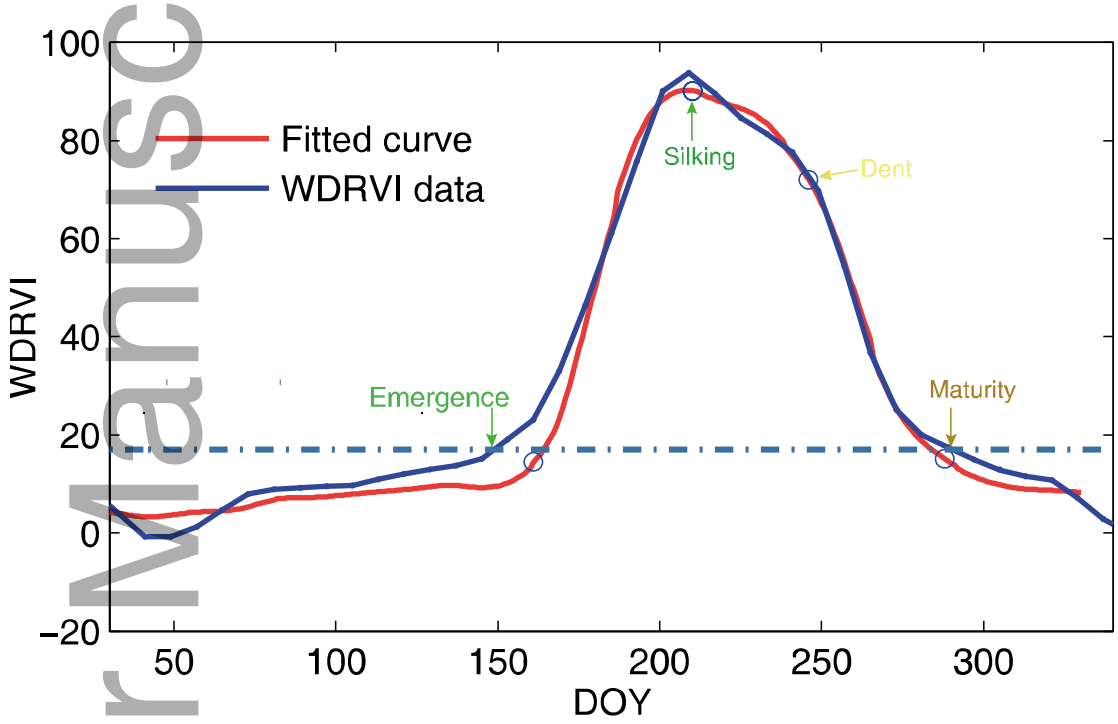

764

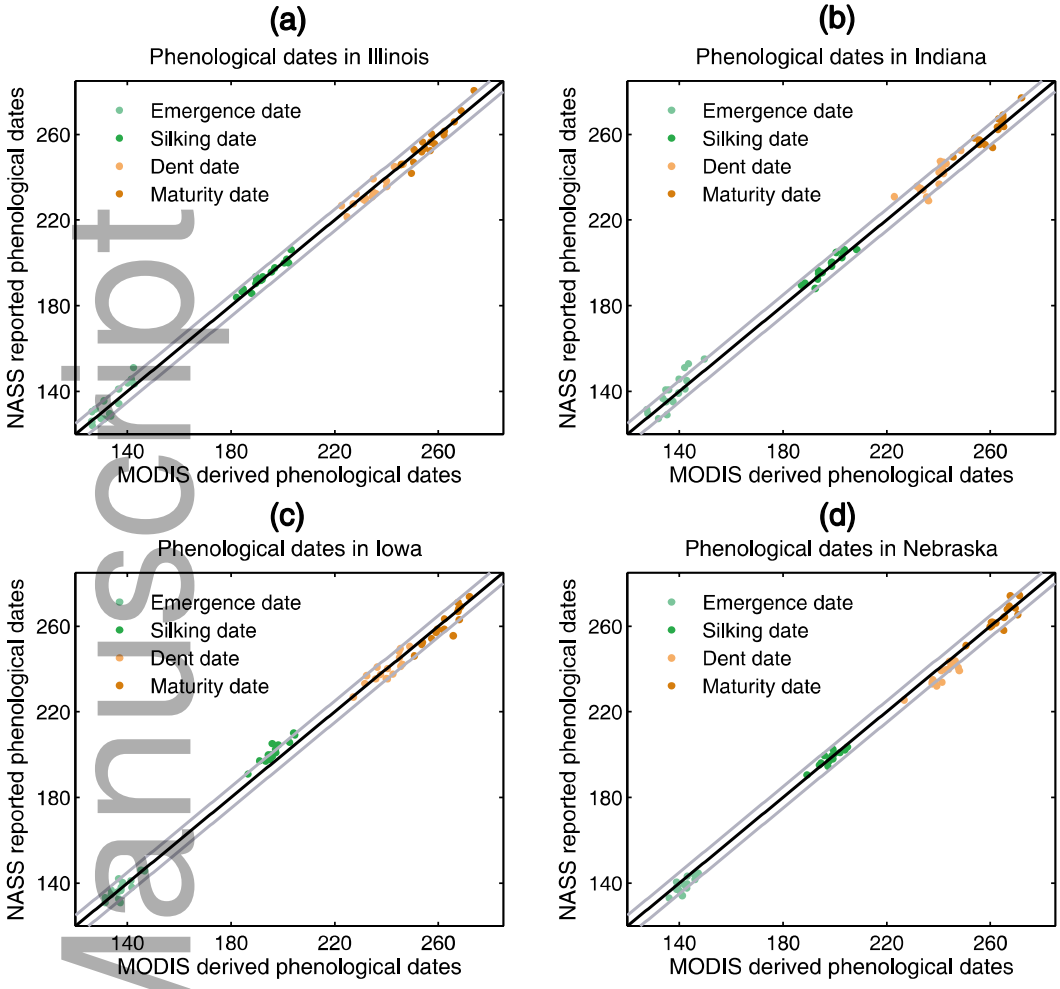

765

766

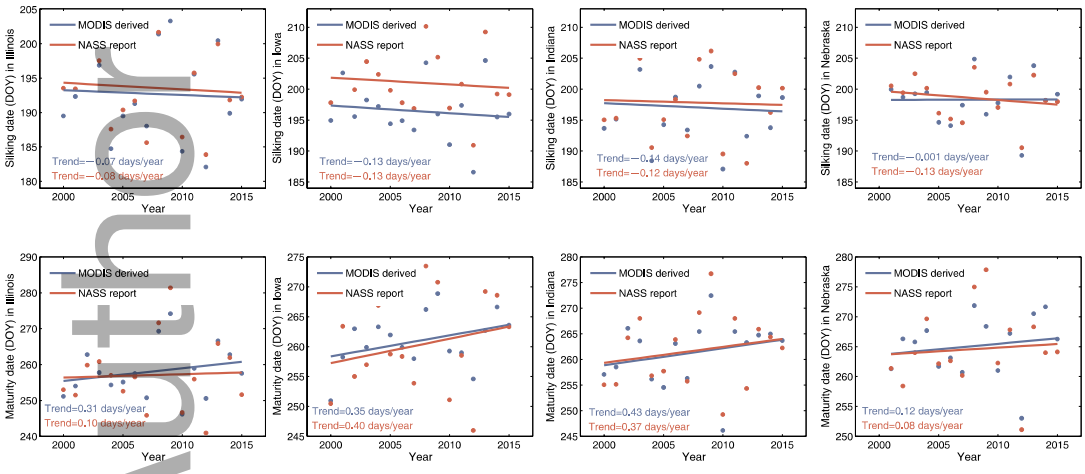

767

768

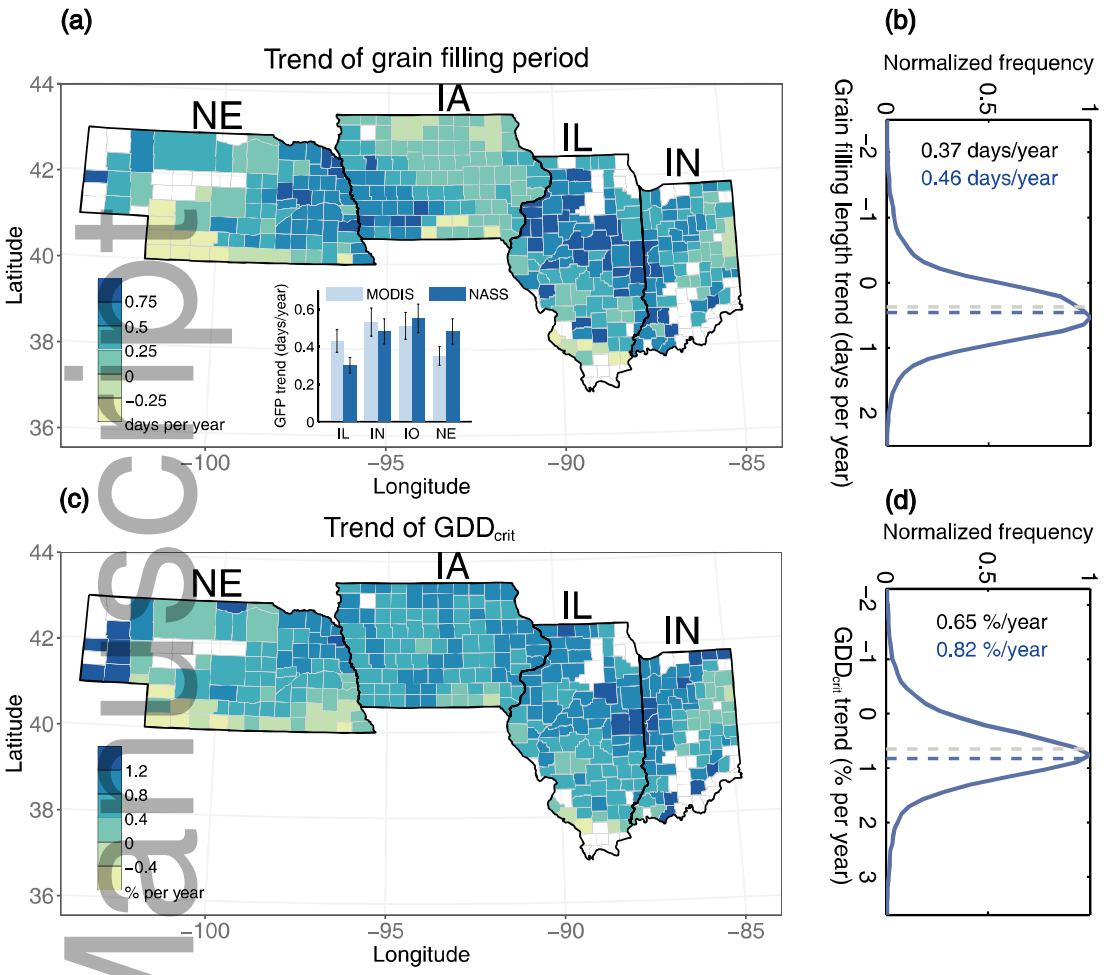

769

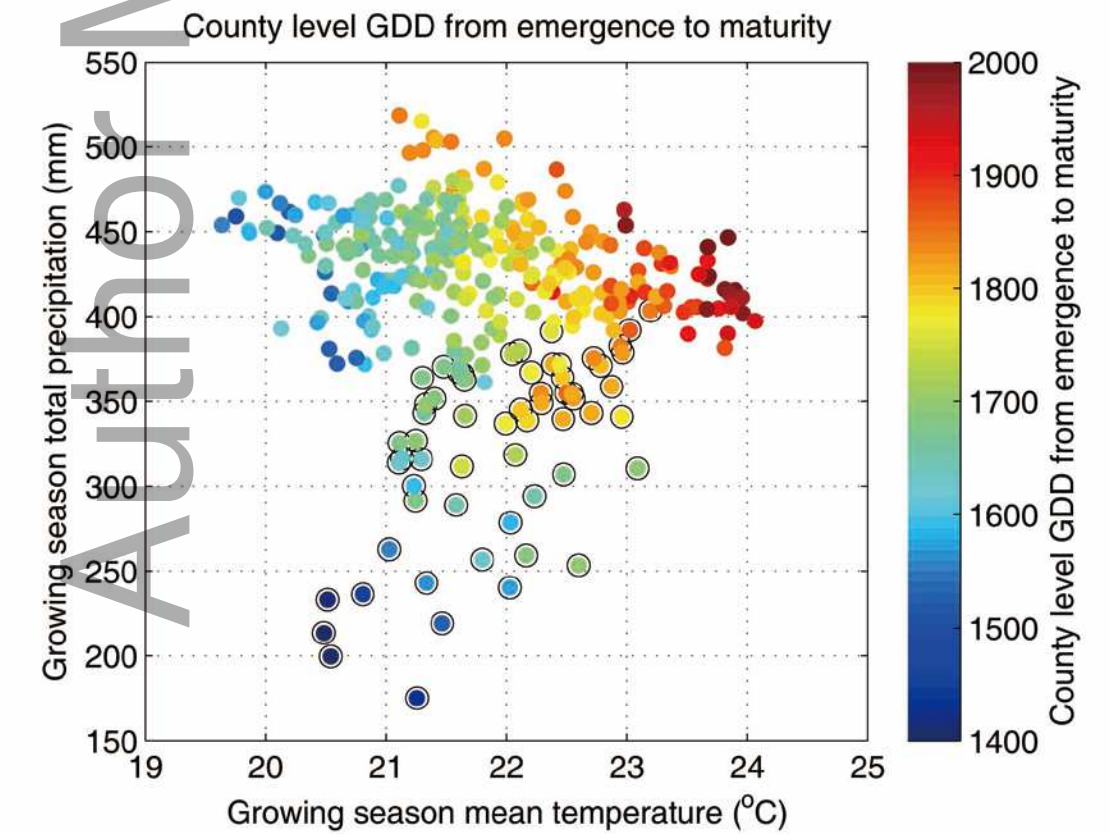

770

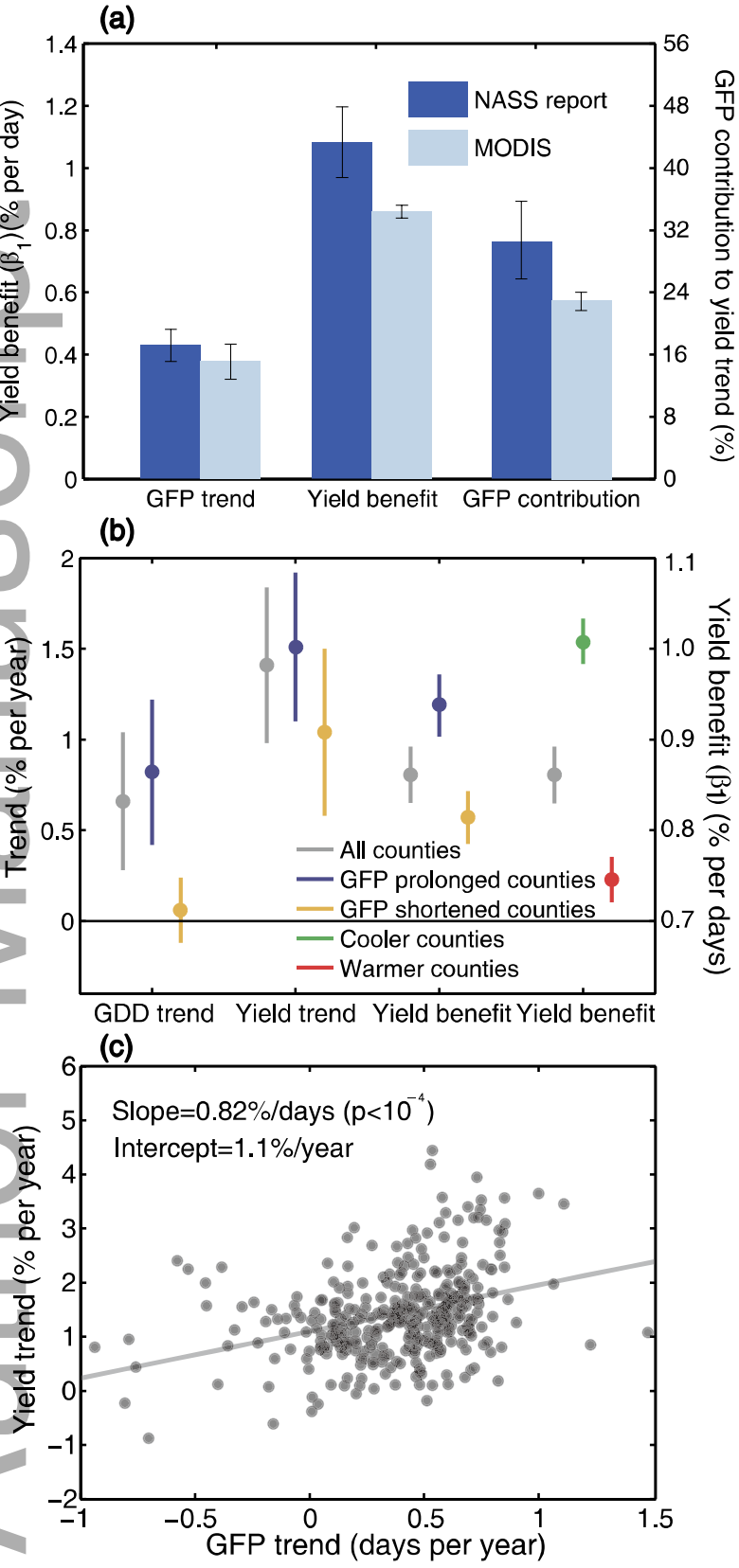

771

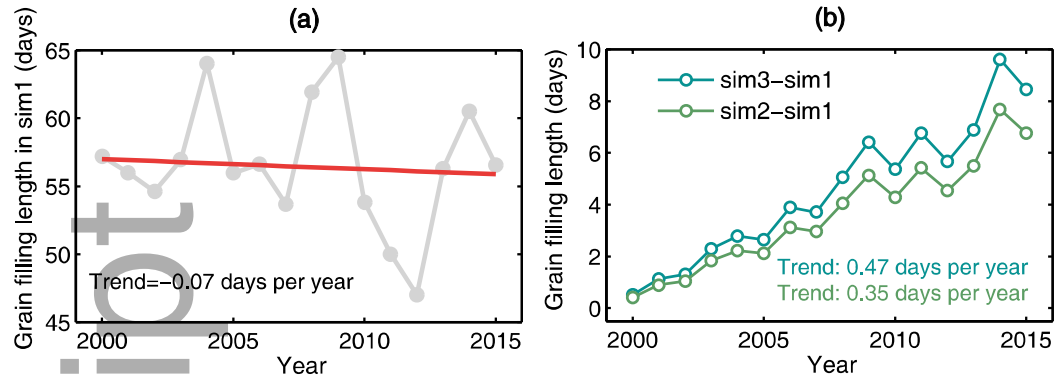

772

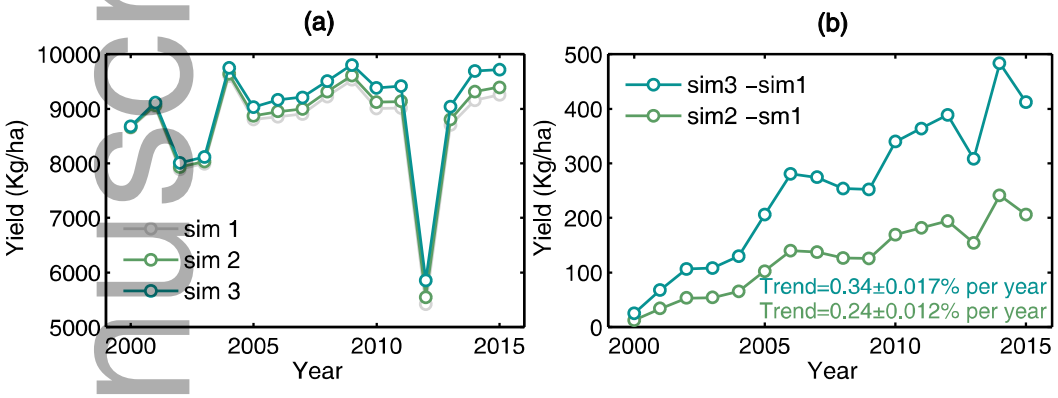

773

774

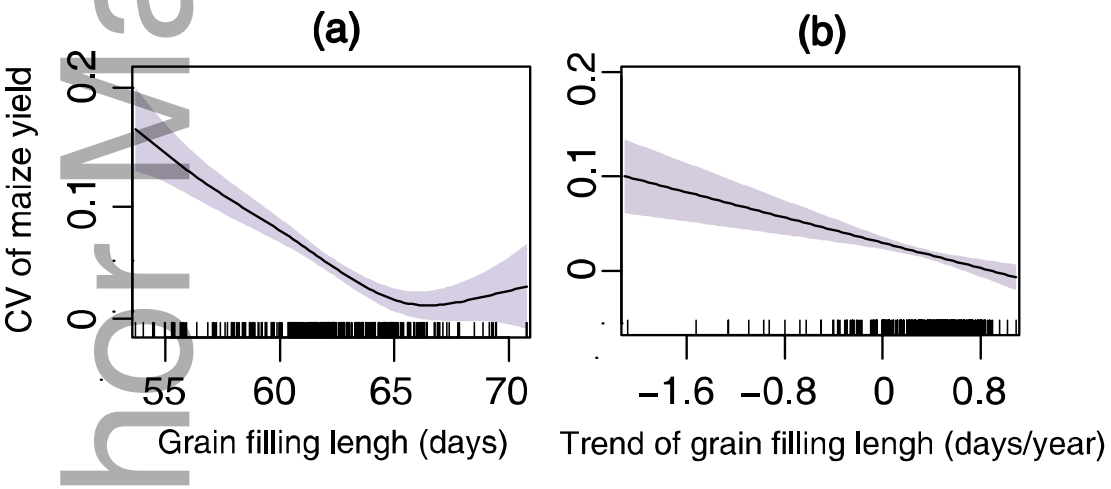

775

776

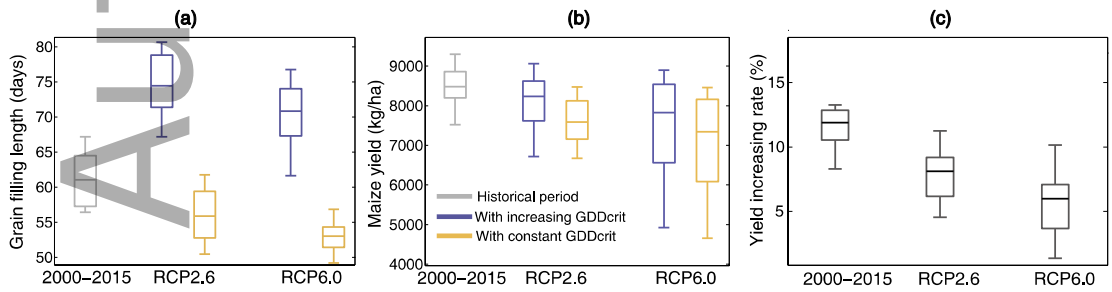

777

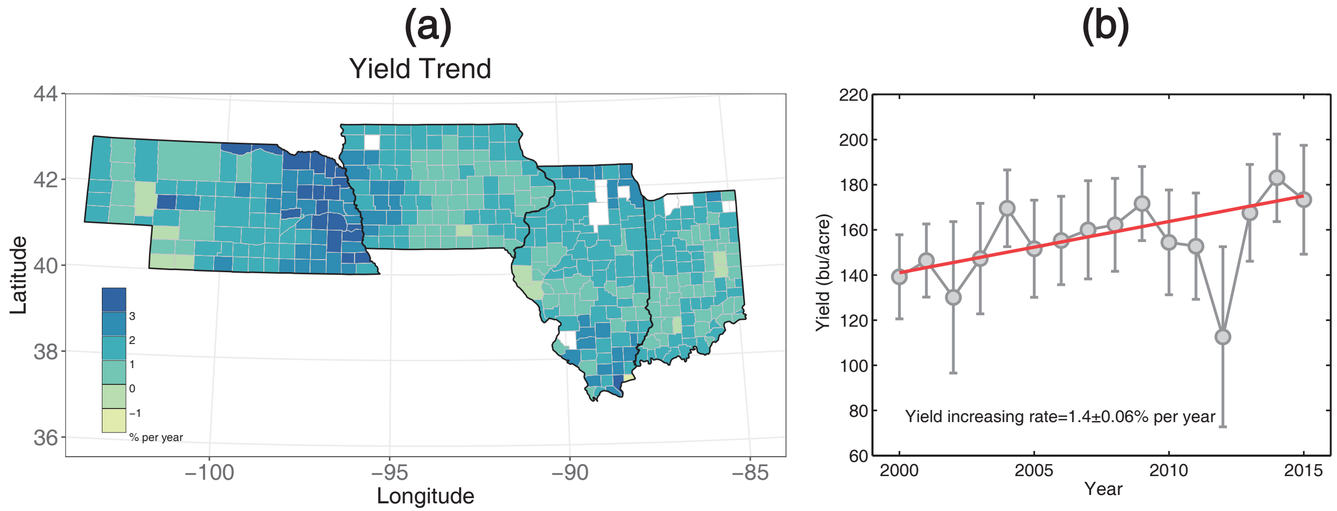

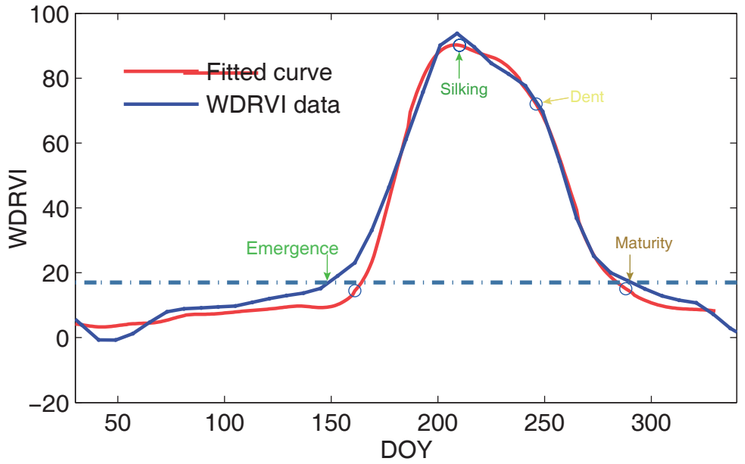

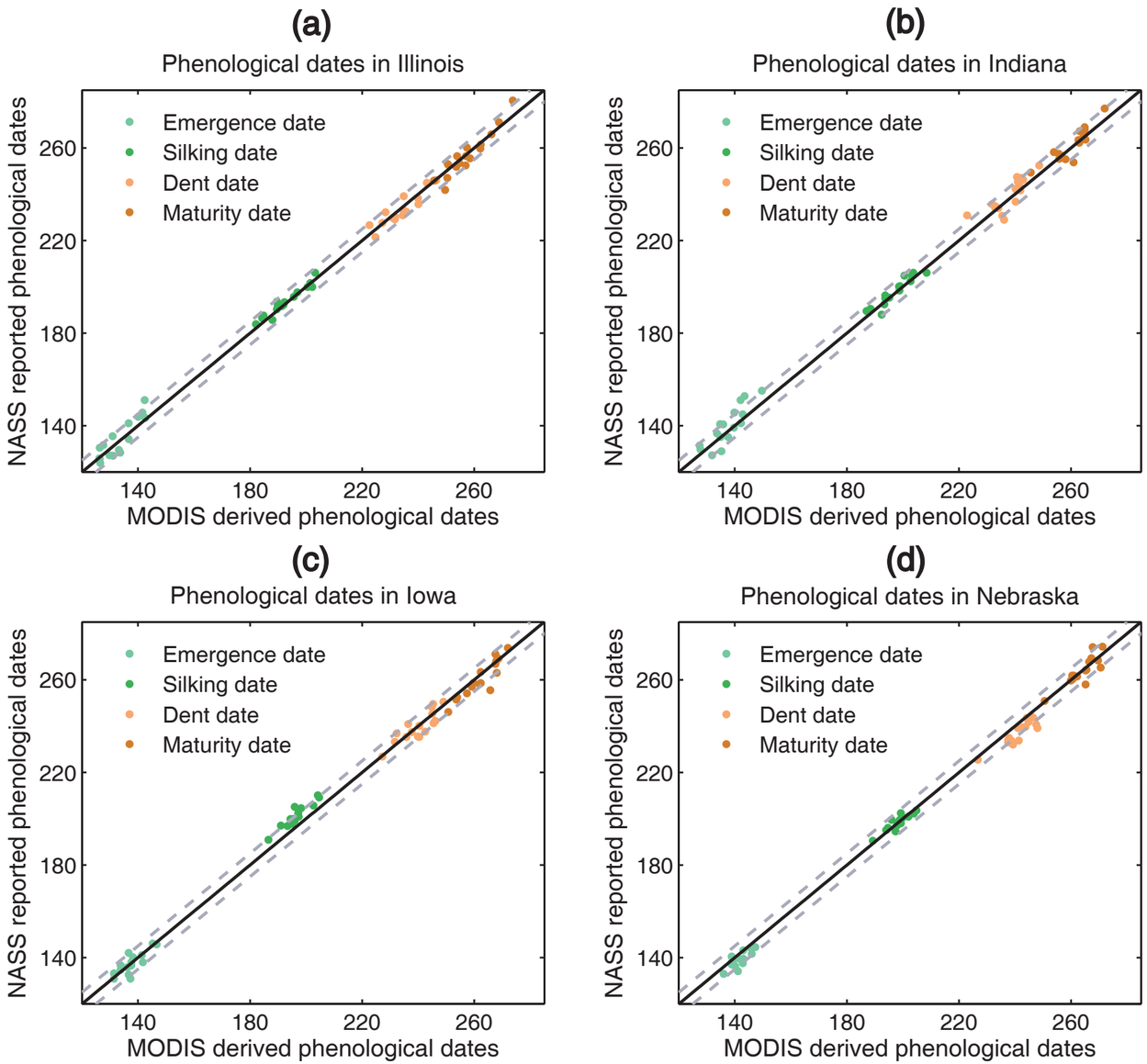

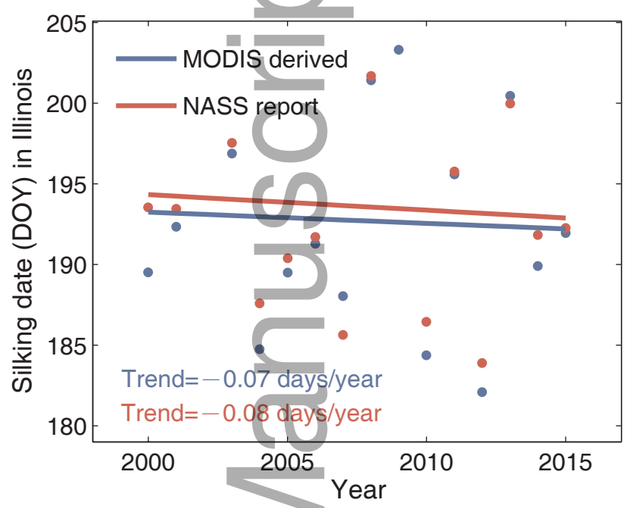

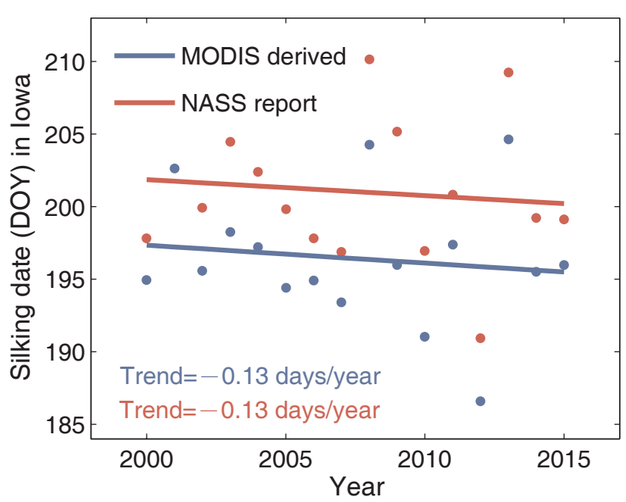

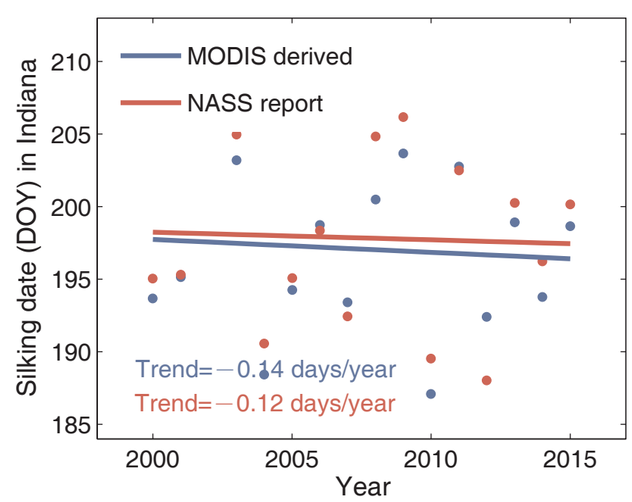

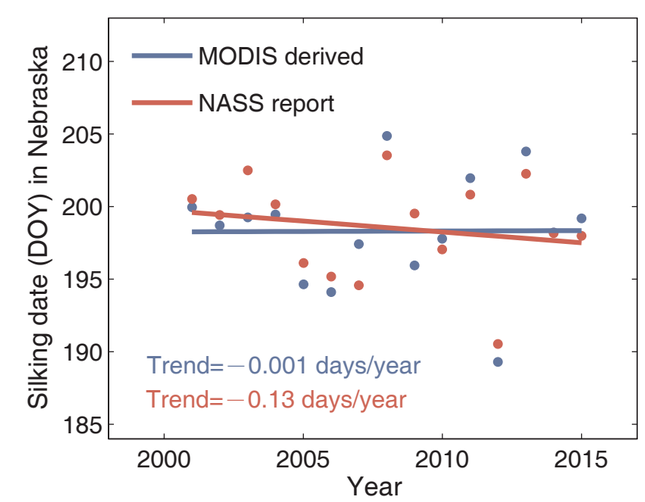

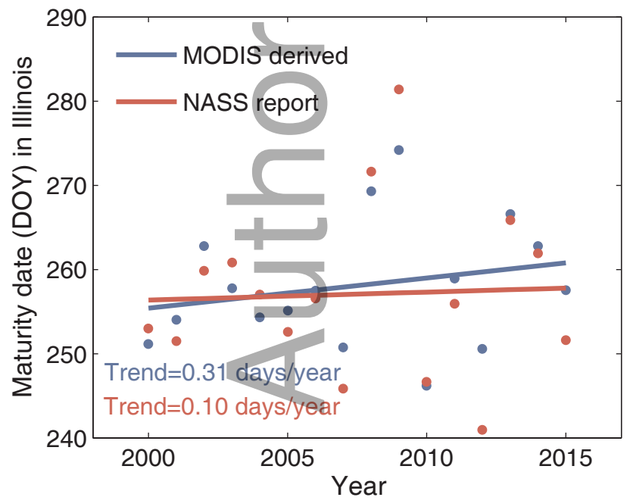

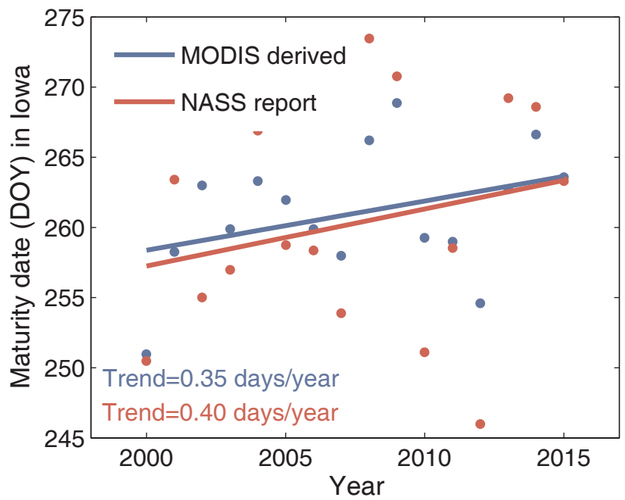

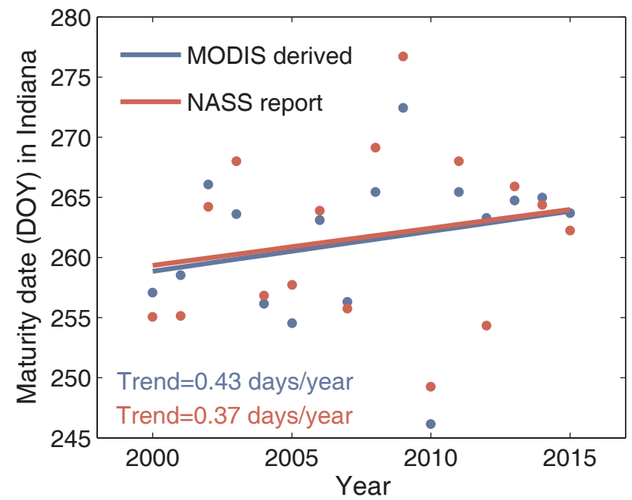

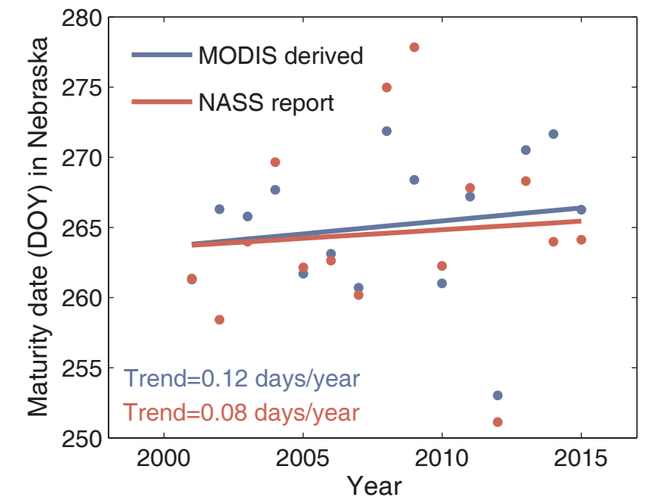

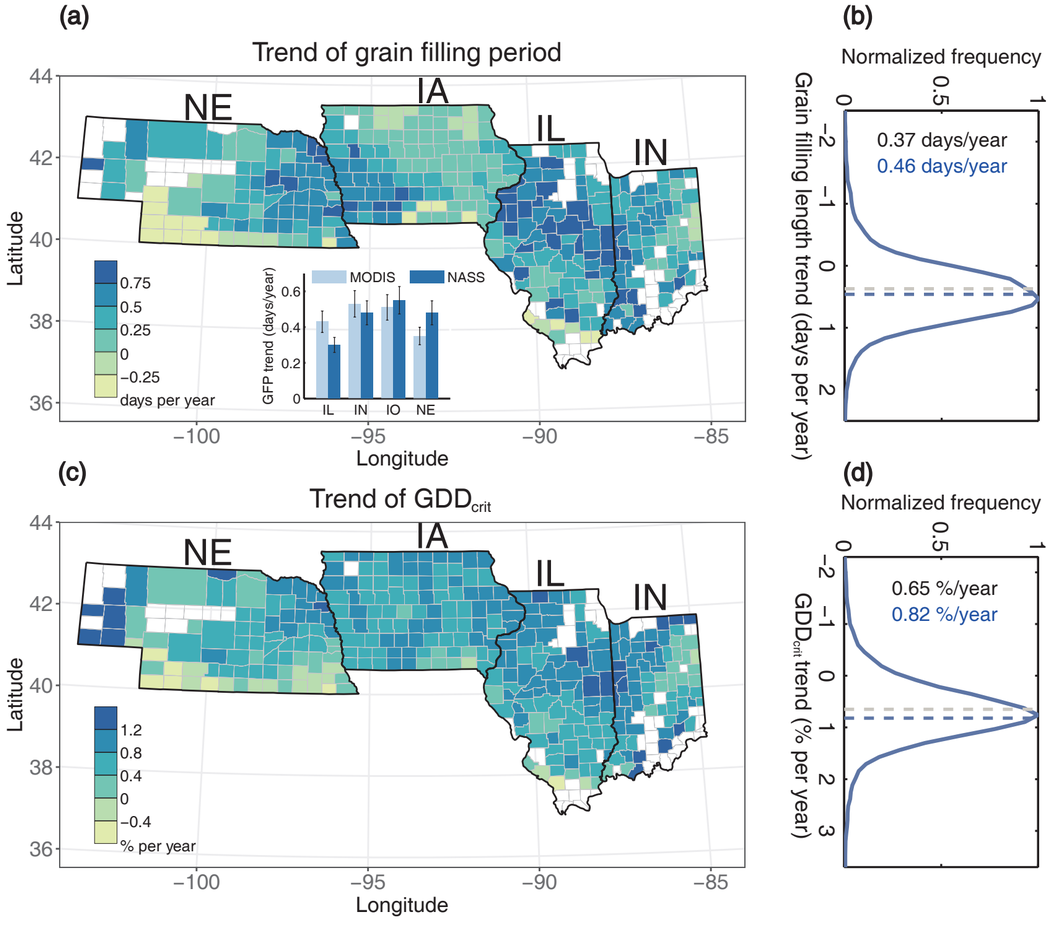

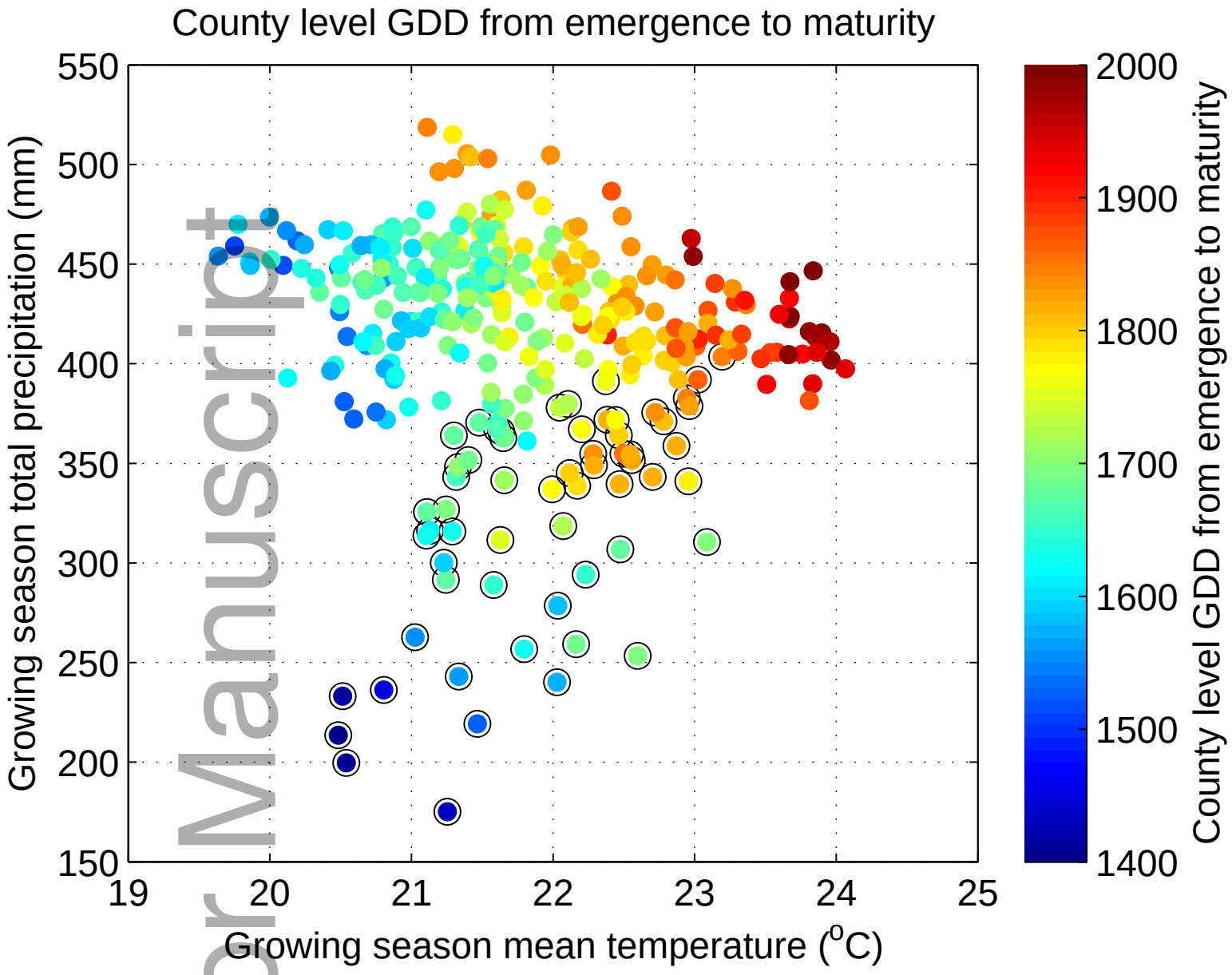

gcb_14356_f6.eps